Chapter 7

GaN and InN Hexagonal Microdisks

Chen-Chi Yang, Ikai Lo, Yu-Chi Hsu and Hong-Yi Yang

Additional information is available at the end of the chapter

http://dx.doi.org/10.5772/intechopen.70120

Abstract

The high-quality GaN microdisks with InGaN/GaN quantum wells (QWs) and InN microdisks were grown on γ-$LiAlO_2$ substrates by plasma-assisted molecular beam epitaxy (PA-MBE). The samples were analysed using scanning electron microscopy, X-ray diffraction, photoluminescence, cathodoluminescence and high-resolution transmission electron microscope. The characteristics of the GaN microdisks and InN microdisks were studied and the effect of growth temperature was evaluated.

Keywords: GaN, InN, microdisk, molecular beam epitaxy

1. Introduction

III-nitride materials have been extensively studied for the applications to high-efficiency lighting sources such as light-emitting diodes (LEDs) or spintronics [1–7]. From the changing of indium content (x), the band-gap of $In_xGa_{1-x}N$ can be tuned from 0.7 to 3.4 eV to cover the whole visible-light spectrum. **Figure 1** shows the diagram of band-gap energies of III-nitrides with bowing parameters [8] versus lattice constants. However, it is difficult to grow high-quality $In_xGa_{1-x}N$/GaN quantum wells (QWs) because of the large lattice mismatch between GaN (a_{GaN} = 0.3189 nm, c_{GaN} = 0.5185 nm) and InN (a_{InN} = 0.35446 nm, c_{InN} = 0.57034 nm) [8, 9]. Furthermore, because of the high volatility of indium atom at high temperature, it is hard to grow a homogenous high-indium-concentration $In_xGa_{1-x}N$/GaN QW thin film by using high-temperature growth techniques (e.g. T > 1000°C) such as vapour phase epitaxy (VPE) or metalorganic chemical vapour deposition (MOCVD). The growth of high-quality $In_xGa_{1-x}N$ epilayer with an indium concentration higher than 20% is regarded as a high challenge [10]. To overcome these difficulties, a plasma-assisted molecular beam epitaxy (PA-MBE) technique was used to grow $In_xGa_{1-x}N$ epilayer at lower temperatures, and some substrates

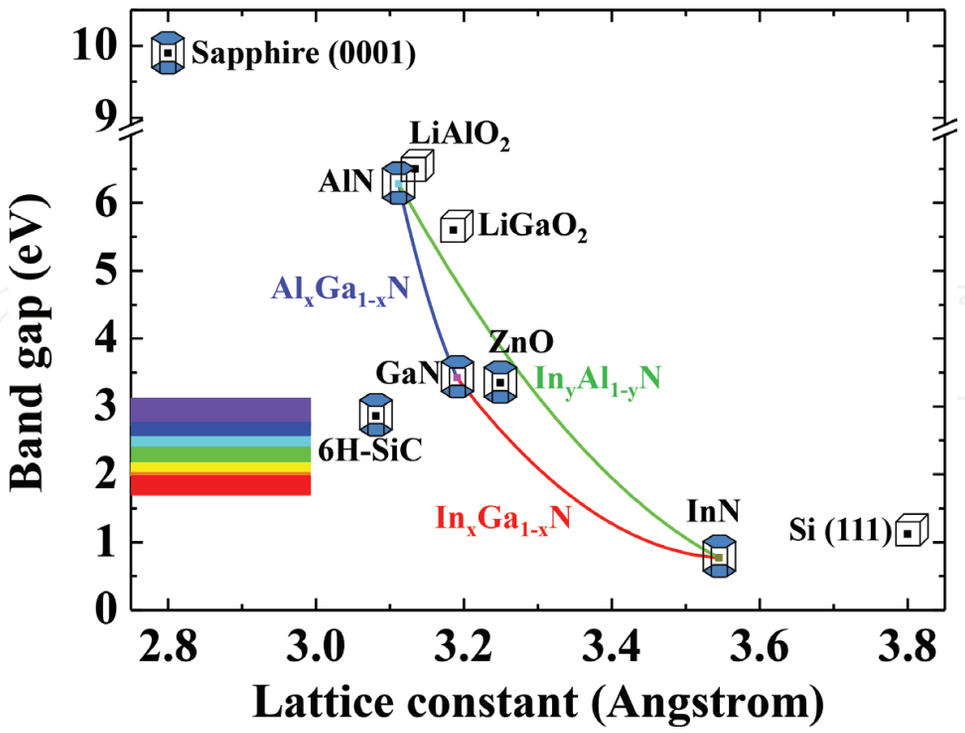

Figure 1. The diagram shows band-gap energies of III-nitrides with bowing parameters versus lattice constants. The substrate materials were also presented.

(such as $LiAlO_2$, $LiGaO_2$, ZnO) were selected to grow GaN epilayers in order to minimize the lattice mismatch between the substrate and GaN layer as compared to the commercial substrates, e.g. sapphire, SiC or Si (1 1 1). From the values of wurtzite GaN on JCPDS files No. 50-0792 and those of γ-$LiAlO_2$ on No. 38-1464, the lattice mismatch between $c/2_{LAO}$ and a_{GaN} is 1.5% indicating that it is suit to grow *c*-plane GaN on the g-$LiAlO_2$ substrate. In this chapter, we show the high-quality epitaxial growth of GaN microdisks with $In_xGa_{1-x}N$/GaN quantum wells and InN microdisks on γ-$LiAlO_2$ lithium aluminium oxide (LAO) substrates at low temperatures by the plasma-assisted molecular beam epitaxy system. Consequently, GaN and InN microdisks provide better opportunities to fabricate the $In_xGa_{1-x}N$/GaN microdisk quantum wells for the application of full-colour micron LED without the sapphire substrate, which is mostly used for the bulk GaN-based quantum wells in commercial LEDs but has a larger lattice mismatch with InN [1, 2].

2. GaN hexagonal microdisks

2.1. Growth of GaN hexagonal microdisks

The sample was grown on a high-quality 1 × 1 cm^2 LAO (1 0 0) substrate by using a low-temperature PA-MBE system (Veeco Applied-GEN 930) with standard effusion cells for Ga-evaporation and an rf-plasma cell with 450 W for N_2-plasma source. The LAO substrate was cut from the crystal ingot, which was fabricated by the traditional Czochralski pulling

http://dx.doi.org/10.5772/intechopen.70120

technique. Before mounting on a holder, the LAO substrate was cleaned with acetone (5 min), isopropanol (5 min) and de-ionized water for a while, and then dried with nitrogen gas immediately. After the chemical cleaning, a thermal treatment was introduced to the LAO substrate in the MBE chamber before epitaxial growth. The LAO substrate was out-gassed at 680°C for 10 min. The temperature was defined by a thermal couple equipped with the backside of the substrate. Thereafter, the substrate temperature was decreased to growth temperatures. The Ga wetting layer was performed on the LAO substrate for 5 min at 630°C, and then the two-step method (i.e. two different N/Ga flux ratios from 28.9 to 139.7, for 35 and 70 min, respectively) was used to fabricate the GaN epi-film at 620°C. The flux ratio was represented by beam equivalent pressure (BEP) of evaporative III-group sources from the standard effusion cell against that of the N_2 source from the rf-plasma cell [11]. In our previous study, we showed the characteristics of *c*-plane GaN (0 0 0$\overline{1}$) hexagonal microdisks [5]. Besides, we developed a back process to fabricate an electrical contact for the GaN hexagonal microdisk on a transparent p-type GaN template [12]. In this chapter, we have consistently grown a sample of GaN microdisks to demonstrate the self-assembling model [5], as shown in **Figure 2**.

2.2. Characteristics of GaN microdisks

The surface morphology of the GaN microdisk sample was evaluated by the field emission scanning electron microscopy (FE-SEM, SII-3050). **Figure 2** shows SEM images with a tilted

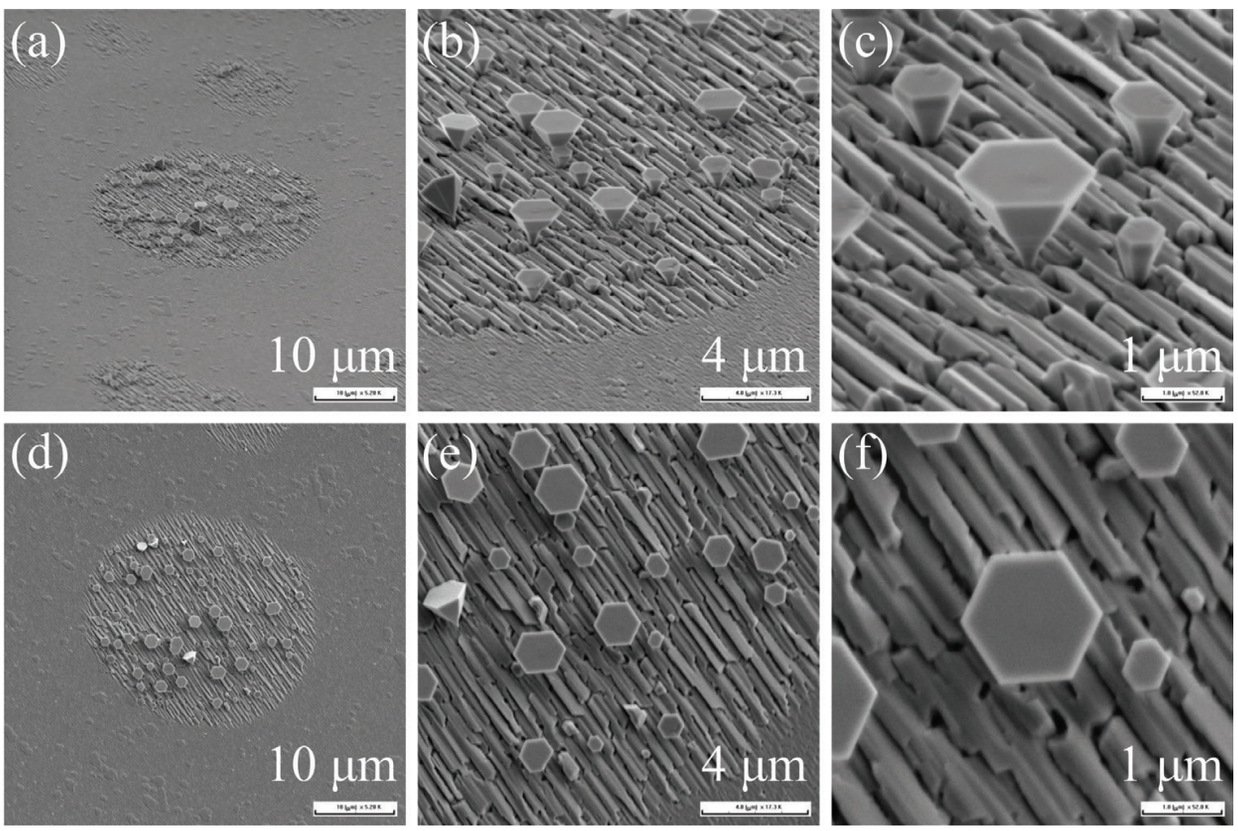

Figure 2. (a)–(c) The tilt-view SEM images of the sample, the scale bars are 10, 4 and 1 μm, respectively. (d)–(f) The top-view SEM images of the sample, the scale bars are 10, 4 and 1 μm, respectively.

angle and a top-view of the sample, respectively. The morphology of the sample exhibited that a two-dimensional (2D) ***M***-plane GaN film and three-dimensional (3D) ***c***-plane GaN hexagonal microdisks were grown on the LAO substrate. The micrographic images of the sample showed that the 2D ***M***-plane GaN epi-film was developed along with the lateral orientation $[1\ 1\ \bar{2}\ 0]_{GaN}$ // $[0\ 0\ 1]_{LAO}$, while the 3D ***c***-plane GaN hexagonal microdisks were grown atop an anionic hexagonal basal plane of LAO. The two-orientation growth of GaN nanopillars on the LAO substrate has been reported in our previous papers [13, 14]. **Figure 2(c)** shows that the neck of contact area between the GaN microdisk and the LAO substrate is small (e.g. less than 200 nm). In addition, the lattice mismatch between $c/2_{LAO}$ and a_{GaN} is only 1.5%. It implies that the GaN microdisk is nearly freestanding as a new substrate for further growth of $In_xGa_{1-x}N$/GaN quantum well (QW) on the top, which ignores the lattice mismatch against the LAO substrate. **Figure 2(f)** shows the enlarged SEM image with a top-view of the GaN hexagonal microdisks shown in the centre of **Figure 2(d)**, and the diameter of the GaN microdisk is about 2.0 μm. Based on the self-assembling model, we will extend to the growth of $In_xGa_{1-x}N$/GaN QW on GaN microdisk and show its characteristics in Section 4.

The optical properties of the GaN microdisk sample were measured by photoluminescence spectroscopy (PL, HORIBA HR800) at room temperature with a light source of He-Cd 325 nm laser. We performed the laser beam focusing on two different spots (S1 and S2) and compared the results with the spot without any microdisk (i.e. mostly ***M***-plane GaN and labelled as background), as shown in **Figure 3**. Two major peaks were obtained for each measurement (S1 or S2). These two major peaks were confirmed by a non-linear Gaussian-function curve fitting with the software Origin (Pro. 8.0). The result of the non-linear Gaussian-function curve fitting showed that the positions of two major peaks for two spots were very consistent. The averaged value for the first peak is (3.385 ± 0.001) eV with the full width at half maximum (FWHM) value equal to (0.128 ± 0.001) eV. It is due to the band-gap transition of wurtzite GaN. The averaged value for the second peak is (2.226 ± 0.003) eV with the FWHM value equal to (0.363 ± 0.033) eV. It is an energy level related to structural defects (e.g. YL in reference [15]) in GaN, so that the FWHM value of GaN is smaller than that of the defect level. The PL intensity corresponding to wurtzite GaN and the defect level indicates that ***c***-plane GaN microdisk is a higher quality structure than ***M***-plane GaN because the intensity of defect level from GaN microdisk is lower than that from ***M***-plane GaN background.

The microstructure of the GaN microdisk sample was analysed by field emission transmission electron microscopy (FE-TEM) (Phillips, model Tecnai F-20) with an electron voltage of 200 kV. The cross-sectional TEM specimen of the sample was prepared by a dual-beam Focus Ion Beam system (FIB, Seiko Inc., SII-3050), on the cleavage plane along the $[1\ \bar{1}\ 0\ 0]$ direction of the ***c***-plane GaN hexagonal microdisk. The FIB was performed with an accelerated voltage of 30 kV to cut the samples roughly and then refined the specimen further by an accelerated voltage of 5 kV. **Figure 4(a)** shows the bright field image with $[1\ 1\ \bar{2}\ 0]_{GaN}$ // $[0\ 0\ 1]_{LAO}$ zone axis. It clearly exhibited that the GaN microdisk was well formed on the LAO substrate. The height for the ***c***-plane GaN hexagonal microdisk from neck to top was about 4.1 μm. The selective area diffraction (SAD) pattern at the top area of the GaN microdisk shown in **Figure 4(b)** clearly showed one single rectangular diffraction pattern at the location of DP01, indicating that the hexagonal microdisk was uniquely formed by the ***c***-plane wurtzite GaN. The ***d***-spacing

http://dx.doi.org/10.5772/intechopen.70120

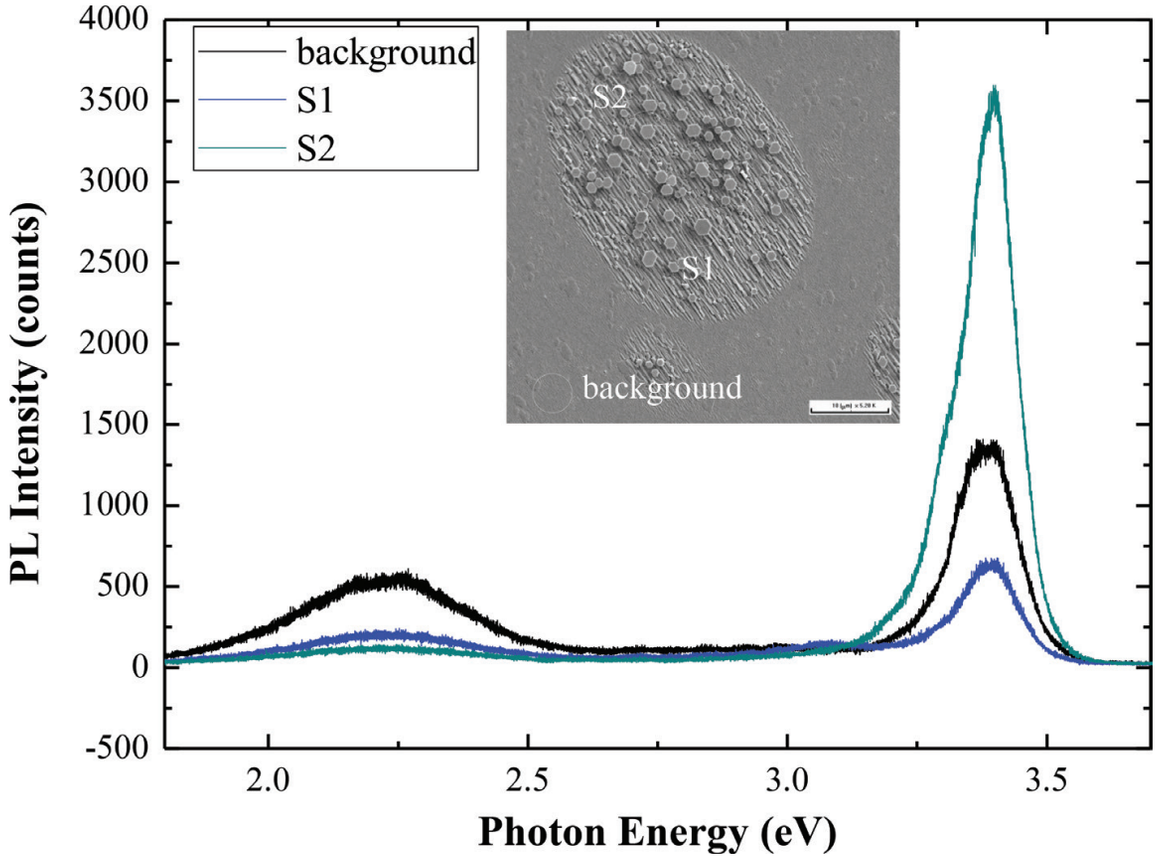

Figure 3. The PL spectra measured at room temperature for different spots (S1 and S2) of the GaN microdisks and ***M***-plane background of the sample.

between the {0 0 0 $\bar{1}$} planes of GaN hexagonal microdisk was measured to be $\boldsymbol{d}_{\mathbf{c}}$ = 0.5254 nm and the ***d***-spacing between the {1 $\bar{1}$ 0 0} planes of GaN hexagonal microdisk was found to be $\boldsymbol{d}_{\mathbf{M}}$ = 0.2785 nm. Compared with the values on JCPDS file No. 50-0792 which are 0.5185 and 0.2762 nm, respectively, the difference between wurtzite GaN microdisk and bulk GaN for $\boldsymbol{d}_{\mathbf{c}}$ and $\boldsymbol{d}_{\mathbf{M}}$ are 1.33 and 0.08%, respectively, revealing that the lattice constant of GaN microdisk is slightly larger than that of bulk GaN. The high-resolution TEM images with the beam direction of $[1\,1\,\bar{2}\,0]_{GaN}$ // $[0\,0\,1]_{LAO}$ were performed at the areas HR01 and HR02 of the sample, as shown in **Figure 4(a)**. The symmetric hexagonal shape reveals the high-quality crystalline structure of the GaN microdisk, as shown in **Figure 4(c)**. The angle between the edge and the growth direction can be examined directly by the high-resolution TEM image performed at HR02 to be about 28°, as shown in **Figure 4(d)**. The ball-stick model for the standard wurtzite GaN (JCPDS file No. 50-0792) with $a = b = 0.3189$, $c = 0.5185$ and $u = \bar{\alpha}/c = 3/8$ was used to simulate the ***c***-plane GaN hexagonal microdisk in **Figure 4(e)**, where blue balls represented Ga atoms and red balls represented N atoms. The ***c***-plane GaN (0 0 0 $\bar{1}$) hexagonal microdisk was built up with the capture of N atoms by the $\bar{\beta}$-dangling bonds of the most-outside Ga atoms and then the capture of Ga atoms by $\bar{\alpha}$-bonds of N atoms to form the microdisk [5]. The lateral over-growth along the (1 $\bar{1}$ 0 0) direction was extended to one $\boldsymbol{d}_{\mathbf{M}}$-spacing for each unit step-layer (i.e. $\boldsymbol{d}_{\mathbf{c}}$-spacing), resulting in the angle of 28° off the ***c***-axis. Based on the ball-stick model, the laterally extensive width along the $[1\,\bar{1}\,0\,0]_{GaN}$ direction per unit step-layer was equal to $\frac{\sqrt{3}}{2}a$. The edge was

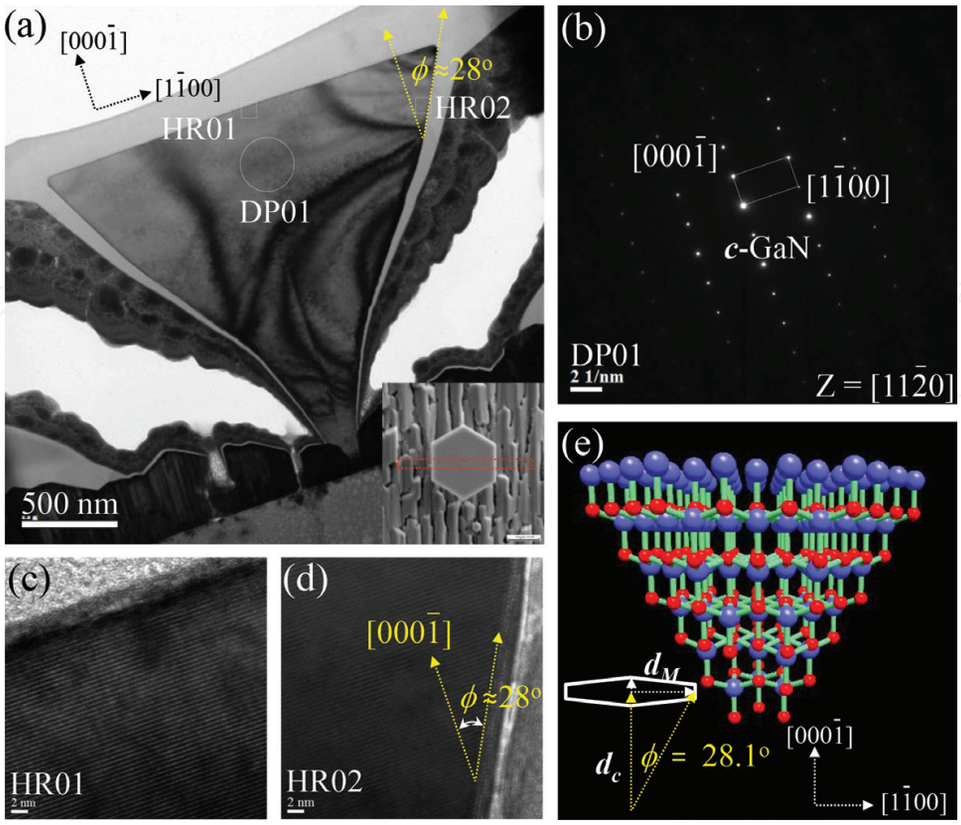

Figure 4. TEM analyses of the GaN hexagonal microdisk: (a) the bright field image with $[1\ 1\ \bar{2}\ 0]_{GaN}$ // $[0\ 0\ 1]_{LAO}$ zone axis. The selective area diffraction patterns taken at the point shown in (a) are presented in (b), the scale bars are 2 (1/nm). The high-resolution TEM images taken at the points shown in (a) are presented in (c) and (d), the scale bars are 2 nm and (e) the ball-stick model for GaN hexagonal microdisk.

then tilted off the ***c***-axis [0 0 0 $\bar{1}$] direction by the angle, $\phi = \tan^{-1}(\frac{\sqrt{3}}{2}a/c) = 28.1°$, where $\frac{\sqrt{3}}{2}a$ is equal to one $d_{M'}$ as shown in **Figure 4(e)**. We also calculated the angle from the measured SAD data at the GaN hexagonal microdisk in **Figure 4(b)**, and obtained that the ***d***-spacing between the {0 0 0 $\bar{1}$} planes was d_c = 0.5254 nm and the ***d***-spacing between the {1 $\bar{1}$ 0 0} planes was d_M = 0.2785 nm, resulting in $\phi = \tan^{-1}(d_M/d_c) = 28.0°$, which was in good agreement with the model predicted. The angle between the edge and the growth direction can be examined directly by the high-resolution TEM image performed at HR02 to be about 28°, as shown in **Figure 4(d)**.

3. InN hexagonal microdisks

3.1. Growth of InN hexagonal microdisks

The two-orientation growth of GaN nanopillars on the LAO substrate has been reported in our previous papers [13, 14] and reconfirmed in Section 2. In this section, we applied the two-orientation growth mechanism to grow the 2D ***M***-plane InN epi-film and 3D ***c***-plane InN hexagonal thin disks on the LAO substrate with the InGaN buffer layer at low growth temperature (470°C). The InN microdisk sample was grown on a high-quality 1 × 1 cm² LAO (1 0 0)

http://dx.doi.org/10.5772/intechopen.70120

substrate with an InGaN buffer layer between them by a low-temperature PA-MBE system (Veeco Applied-GEN 930). The LAO substrate was cut from the crystal ingot, which was fabricated by the traditional Czochralski pulling technique. The growth details were described completely in our previous paper which was published in *AIP Advances* [16].

3.2. Characteristics of InN microdisks

The crystal structure of the InN microdisk sample was characterized by the high-resolution X-ray diffraction (XRD; Bede D1) measurement and is shown in **Figure 5(a)**. From the result of X-ray diffraction pattern (i.e. the peak at 2θ = 31.69°), we estimated the indium content of $In_xGa_{1-x}N$ on the basis of Vegard's law to be about 20% [17]. The peaks at 2θ = 29.07, 31.31, 32.29 and 34.69° represented the X-ray diffraction patterns from the ***M***-plane InN (1 $\bar{1}$ 0 0), ***c***-plane InN (0 0 0 $\bar{2}$), ***M***-plane GaN (1 $\bar{1}$ 0 0) and LAO (1 0 0), respectively. These peak positions at the X-ray diffraction patterns were obtained and matched with those data of the standard wurtzite structure bulk InN (JCPDS file No. 50-1239) by the asymmetric double sigmoidal linear curve fitting with the software Quick Graph (Version 2.0). The ***d***-spacing between the {0 0 0 $\bar{2}$} planes of InN was evaluated to be d_{0002} = 0.28216 nm from the Bragg's law ($2d\sin\theta = n\lambda$) with Cu $K_{\alpha 1}$ wavelength λ = 0.1540562 nm. The lattice constant of wurtzite InN microdisk is smaller than that of bulk InN by comparing with the value on JCPDS file, d_{0002} = 0.28528 nm, and the difference between InN microdisk and bulk InN is 1.09%.

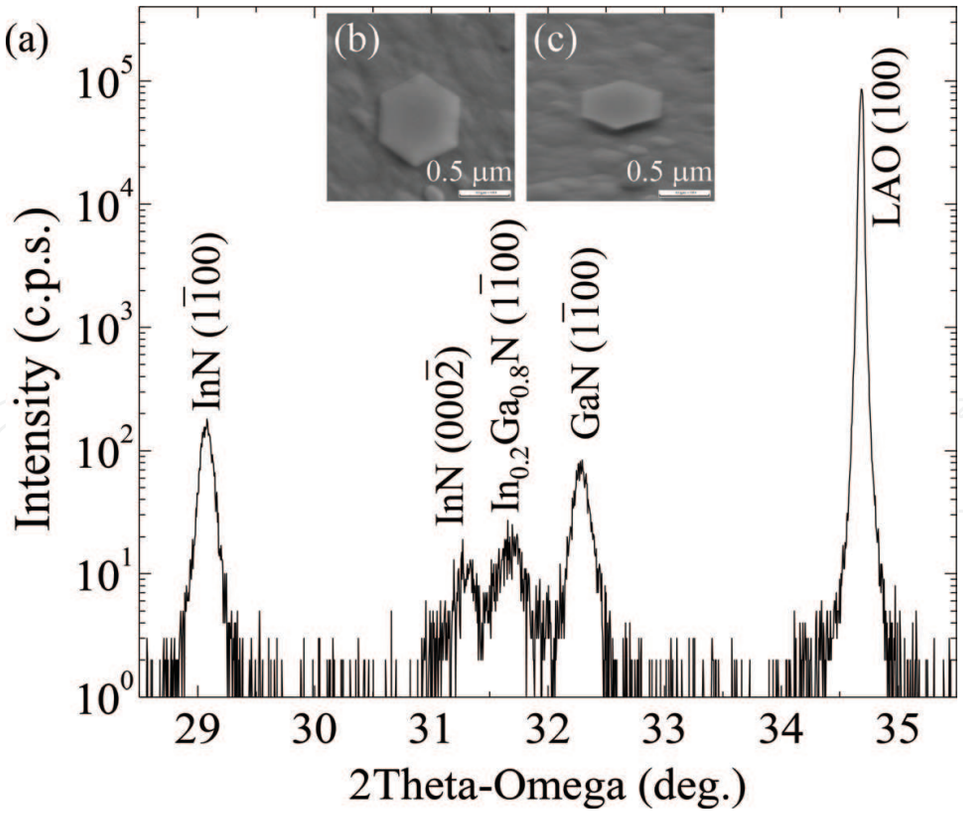

Figure 5. (a) The X-ray 2Theta-Omega scan of the sample. (b) The top-view SEM image of InN hexagonal thin disk, the scale bar is 0.5 μm. (c) The tilt-view SEM image of InN hexagonal thin disk, the scale bar is 0.5 μm.

The surface morphology of the InN microdisk sample was evaluated by the field emission scanning electron microscopy (FE-SEM, SII-3050). **Figure 5(b)** shows the top-view SEM image of the sample, and the diameter of the InN microdisk was about 0.96 μm. The morphology of the sample exhibited that 2D ***M***-plane InN epi-film and 3D ***c***-plane InN hexagonal microdisks were grown on the LAO substrate. **Figure 5(c)** shows the tilt-view SEM image of the InN microdisk. The micrographic images of the sample showed that the 3D ***c***-plane InN hexagonal microdisks and nanopillars were grown atop an anionic hexagonal basal plane of LAO, while the 2D ***M***-plane InN epi-film was developed along with the lateral orientation $[1\ 1\ \bar{2}\ 0]_{InN}$ // $[0\ 0\ 1]_{LAO}$. Compared with the shape of GaN microdisk, InN microdisk was thinner than GaN microdisk.

The microstructure of the sample was analysed by field emission transmission electron microscopy (FE-TEM) (Phillips, model Tecnai F-20) with an electron voltage of 200 kV. The cross-sectional TEM specimen of the sample was prepared by a dual-beam FIB system (Seiko Inc., SII-3050), on the cleavage plane along the $[1\bar{1}\ 0\ 0]$ direction of the *c*-plane InN hexagonal thin disk. The FIB was performed with an accelerated voltage of 30 kV to cut the samples roughly and then refined the specimen further by an accelerated voltage of 5 kV. **Figure 6(a)** shows the bright field image with the $[1\ 1\bar{2}\ 0]_{InN}$ // $[0\ 0\ 1]_{LAO}$ zone axis. It clearly exhibited that InN was well-formed on the InGaN buffer layer, and the InGaN buffer layer was well-established on the GaN epi-layer. The thicknesses of ***M***-plane InN, ***M***-plane InGaN and ***M***-plane GaN were measured to be about 265, 51 and 137 nm, respectively. The height for the ***c***-plane InN hexagonal thin disk from neck to top was about 188 nm. The *c*-plane wurtzite structure was followed up to the neck area and formed a uniform *c*-plane InGaN pyramid-shaped structure. Outside the pyramid-shaped structure, the wave-shaped structures were produced by the staking faults between the misfit *c*-plane wurtzite structures of InGaN and InN. The wave-shaped structures became uniform and then the *c*-plane wurtzite structure was followed further to form the InN hexagonal microdisk. The selective area diffraction (SAD) pattern at the top area of hexagonal thin disk shown in **Figure 6(b)** clearly showed one single rectangular diffraction pattern at the location of DP01, indicating that the hexagonal thin disk was uniquely formed by the ***c***-plane wurtzite InN. The ***d***-spacing between the $\{0\ 0\ 0\ \bar{1}\}$ planes of InN hexagonal thin disk was measured to be $\boldsymbol{d}_c$ = 0.5687 nm and the ***d***-spacing between the $\{1\bar{1}\ 0\ 0\}$ planes of InN hexagonal thin disk was $\boldsymbol{d}_M$ = 0.3025 nm. Compared with the values on JCPDS file No. 50-1239, which are 0.5703 and 0.30647 nm, respectively, the difference between wurtzite InN microdisk and bulk InN for $\boldsymbol{d}_c$ and $\boldsymbol{d}_M$ are 0.28 and 1.24%, respectively, revealing that the lattice constant of wurtzite InN microdisk is smaller than that of bulk InN. The angle between edge and growth direction can be examined directly by the high-resolution TEM image performed at HR01 to be about 73°, as shown in **Figure 6(c)**. To establish the growth mechanism of the thin InN hexagonal microdisk, we demonstrated a ball-stick model for the self-assembled thin InN microdisk. The ball-stick model for the standard wurtzite InN (JCPDS file No. 50-1239) with $a = b = 0.3537$, $c = 0.5703$ and $u = \overline{\alpha}/c = 3/8$ was used to simulate the *c*-plane InN hexagonal microdisk, as shown in **Figure 6(d)** and **(e)**, where blue balls represented In atoms and red balls represented N atoms. In the case of InN thin disk, when the growth temperature lowered to 470°C, the ***c***-plane InN $(0\ 0\ 0\ \bar{1})$ hexagonal thin disk was built up with the capture of N atoms by the $\overline{\beta}$-dangling bonds of the most-outside In atoms and then the lateral over-growth occurred; and the capture of In atoms by $\overline{\beta}$-dangling bonds of N atoms to form

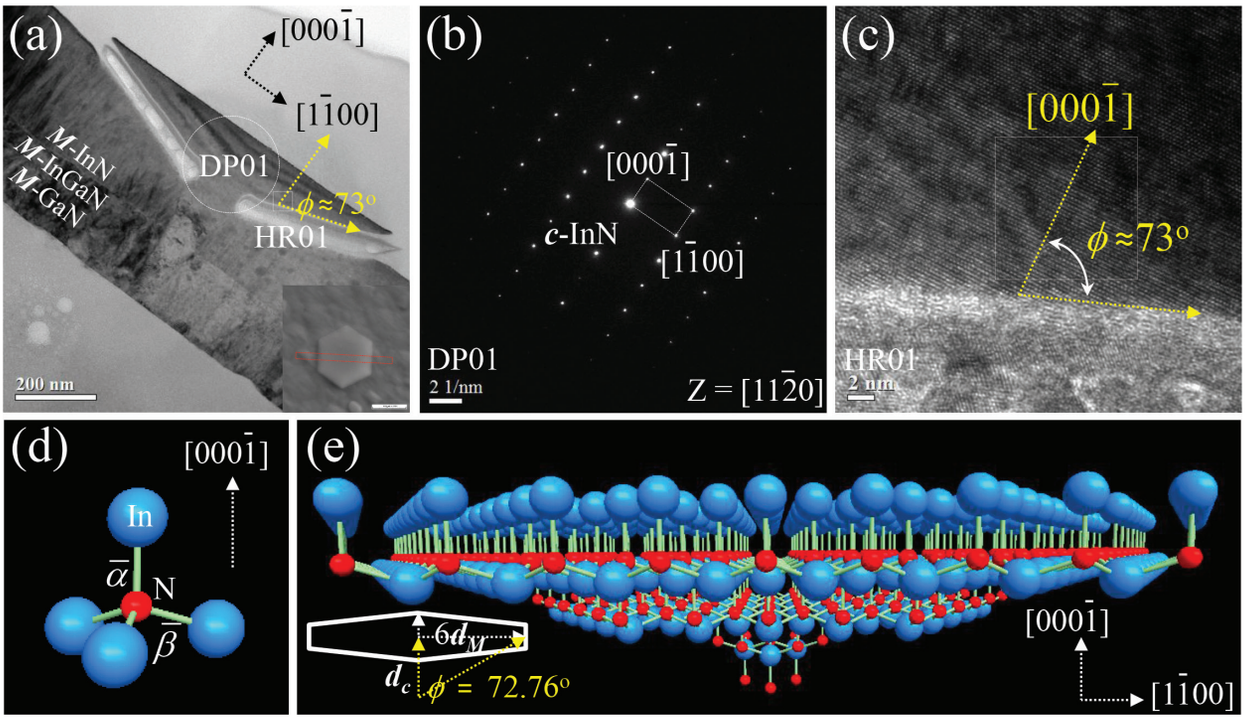

Figure 6. TEM analyses of the InN hexagonal thin disk: (a) the bright field image with $[1\,1\,\bar{2}\,0\,1]_{InN}$ // $[0\,0\,1]_{LAO}$ zone axis. The selective area diffraction patterns taken at the points shown in (a) are presented in (b), the scale bars are 2 (1/nm). The high-resolution TEM images taken at the point shown in (a) are presented in (c), the scale bars are 2 nm. The ball-stick model for InN epilayer: (d) the chemical bonds of the $(0\,0\,0\,\bar{1})$ surface and (e) the hexagonal thin disk.

the thin microdisk. The lateral over-growth along the $(1\bar{1}\,0\,0)$ direction was extended to six d_M-spacings for each unit step-layer (i.e. d_c-spacing), resulting in the angle of 73° off the *c*-axis. Based on the ball-stick model, the laterally extensive width along the $[1\bar{1}\,0\,0]_{InN}$ direction per unit step-layer was equal to $3\sqrt{3}\,a$. The edge was then tilted off the *c*-axis $[0\,0\,0\,\bar{1}]$ direction by the angle, $\phi = \tan^{-1}(3\sqrt{3}\,a/c) = 72.76°$, where $3\sqrt{3}\,a$ is equal to $6d_M$, as shown in **Figure 6(e)**. We also calculated the angle from the measured SAD data at the InN hexagonal thin disk in **Figure 6(b)**, and obtained that the *d*-spacing between the $\{0\,0\,0\,\bar{1}\}$ planes was $d_c = 0.5687$ nm and the *d*-spacing between the $\{1\bar{1}\,0\,0\}$ planes was $d_M = 0.3025$ nm, resulting in $\phi = \tan^{-1}(6d_M/d_c) = 72.60°$, which was in good agreement with the model predicted (**Table 1**).

4. InGaN/GaN quantum well

4.1. Growth

The growth mechanism of the awl-shaped GaN microdisk is divergently self-assembled, indicating that the hexagonal neck area for initial nucleation between GaN microdisk and LAO substrate is very small (diameter ~100 nm), and the strain due to the lattice-mismatch between GaN and LAO substrate will not be delivered to the awl-shaped GaN microdisk at the top. This is the way that the GaN microdisk can be grown in balance with a good awl-shape of

	Growth temperature	Growth mechanism (lateral over-growth)	Oblique angle	Application
GaN microdisk	620°C	One d_M/d_c	28°	Base for InGaN/GaN QW
InN microdisk	470°C	Six d_M/d_c	73°	Base for InGaN/GaN QW

Table 1. Comparison of properties of GaN and InN microdisks.

hexagonal disk. The experimental results revealed that the awl-shaped GaN microdisk exhibited a high-quality single crystal. Therefore, the awl-shaped GaN microdisk can be regarded as a nearly freestanding substrate (strain-free) to grow the $In_xGa_{1-x}N$/GaN multiple quantum wells (MQWs) on its top. The $In_xGa_{1-x}N$/GaN double quantum well (DQWs) microdisk sample was grown on a high-quality 1 × 1 cm^2 LAO (1 0 0) substrate by low-temperature PA-MBE system (Veeco Applied-GEN 930). The LAO substrate was cut from the crystal ingot, fabricated by the traditional Czochralski pulling technique. The growth details were described completely in our previous paper which was published in *Applied Physics Letters* [18].

4.2. Characteristics of InGaN/GaN microdisks

The surface morphology of the InGaN/GaN microdisk sample was evaluated by the field emission scanning electron microscopy (FE-SEM, SII-3050). **Figure 7** shows SEM images with a tilted-angle view and a top view of the sample, respectively. The surface morphology of the sample was formed by the two-orientation growth mechanism. Comparing with the surface morphology of GaN microdisks, the shape of the as-grown InGaN/GaN DQW microdisks still maintains the hexagonal shape. **Figure 7(f)** shows the enlarged SEM image with a top view of the GaN hexagonal microdisk, which is shown in the centre of **Figure 7(d)**, and the diameter of the centre GaN microdisk is about 1.96 μm.

The optical properties of the sample were measured by photoluminescence (PL, HORIBA HR800) at room temperature with a light source of He-Cd 325 nm laser. We performed the laser beam focusing on three different spots (S1–S3) and compared the results with the spot without any microdisk (i.e. mostly ***M***-plane GaN and labelled as background), as shown in **Figure 8**. Two major peaks were obtained for each measurement (S1–S3). These two major peaks were confirmed by a non-linear Gaussian-function curve fitting with the software Origin (Pro. 8.0). The result of the non-linear Gaussian-function curve fitting showed that the positions of two major peaks for three spots were very consistent. The averaged value for the first peak is (2.199 ± 0.001) eV with the FWHM value equal to (0.410 ± 0.005) eV. It is due to the band-gap transition of InGaN wells. According to Vegard's law [19] with the bowing effect of bulk $In_xGa_{1-x}N$: $E_g(x) = [3.42 - x*2.65 - x*(1 - x)*2.4]$ eV [8], we estimated the content of indium in the $In_xGa_{1-x}N$ DQWs, which is found to be about 28%. We note that the bowing factor needs to be modified slightly for a quantum well, and the energy-shift due to the quantum confinement will also result in a small deviation to the indium concentration of the $In_xGa_{1-x}N$/GaN DQWs. The averaged value for the second peak is (3.380 ± 0.001) eV with

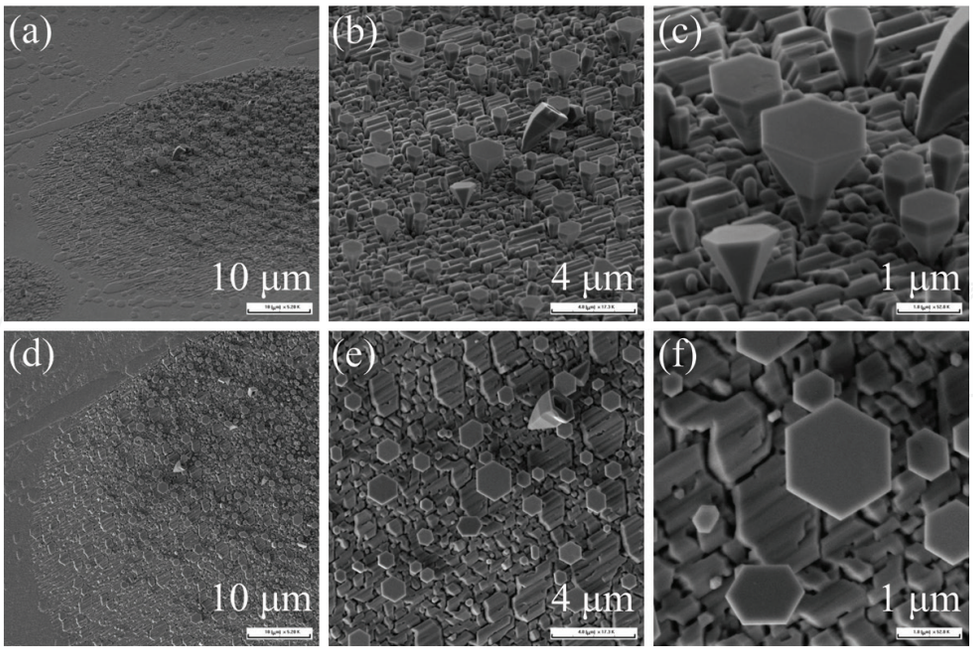

Figure 7. (a)–(c) The tilt-view SEM images of the sample, the scale bars are 10, 4 and 1 μm, respectively. (d)–(f) The top-view SEM images of the sample, the scale bars are 10, 4 and 1 μm, respectively.

the FWHM value equal to (0.043 ± 0.001) eV. It is due to the band-gap transition of wurtzite GaN. The FWHM value of GaN is smaller than that of $In_xGa_{1-x}N$ QDWs because the defect density in GaN is much less than that in InGaN. The PL intensity from $In_xGa_{1-x}N$ quantum wells is higher than that from GaN due to the effect of quantum confinement. It also dominates the PL spectrum of background area tremendously.

An $In_xGa_{1-x}N$/GaN microdisk was used to evaluate the details of light-emitting area by cathodoluminescence (CL, JEOL JSM-6330) and secondary electron images (SEI) measurements. The result of CL measurement is shown in **Figure 9**. We obtained the CL spectrum by detecting the photon energy from 700 (e.g. 1.77 eV) to 340 nm (e.g. 3.64 eV) with an accelerative voltage of 10 kV and an extraction voltage of photon-electric magnitude tube of 1100 V. Under such a condition, we observed two major peaks at (2.221 ± 0.0001) eV with the FWHM value equal to (0.182 ± 0.001) and (3.398 ± 0.0001) eV with the FWHM value equal to (0.046 ± 0.001) eV. We also observed the smallest peak at (2.805 ± 0.002) eV with the FWHM value equal to (0.110 ± 0.001) eV. The insets of **Figure 9** show the CL images corresponding to the three peak energies. The CL images show that the peak for the wavelength of 364 nm (e.g. 3.407 eV) is mainly emitted from wurtzite GaN microdisks. The peak for the wavelength of 560 nm (e.g. 2.214 eV) is the highest peak and mainly emitted from the $In_xGa_{1-x}N$ quantum wells in the $In_xGa_{1-x}N$/GaN microdisks. We also observed the edge of microdisk is brighter than the central area. It might arise from the enhanced emission by total internal reflection in the DQWs structure [20]. The optical properties of these two major peaks are consistent with the results of PL spectra, but the smallest peak for the wavelength of 450 nm (e.g. 2.756 eV) is not observed in the PL spectra. The peak at 2.805 eV was attributed to the energy level related to the structural defects (e.g. Y_{10} in reference [15]) in microdisks.

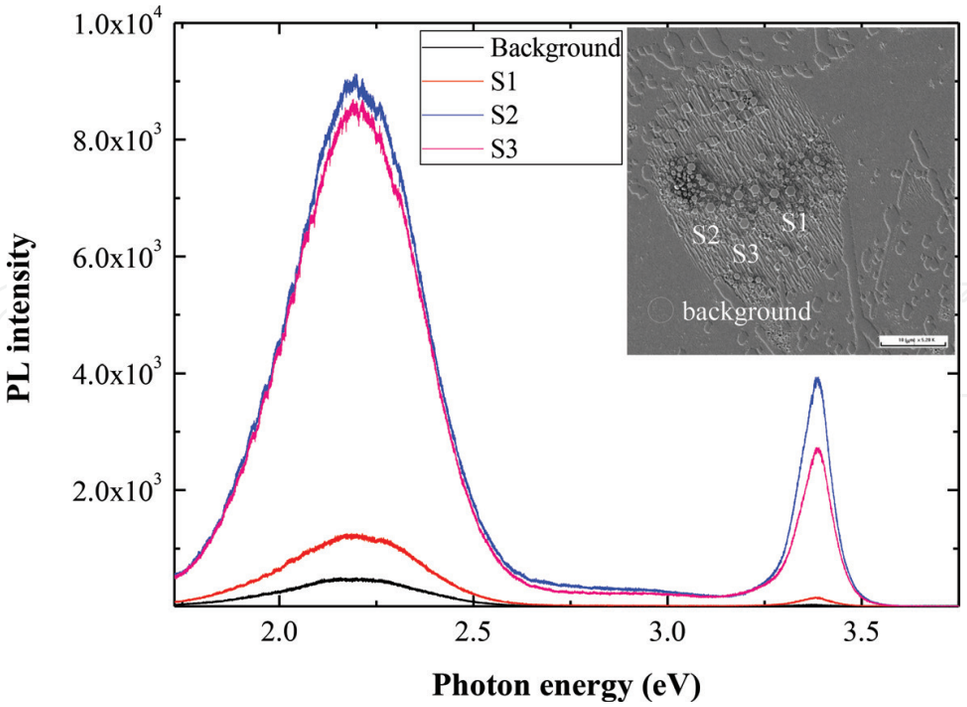

Figure 8. The PL spectra measured at room temperature for different spots (S1–S3) of the $In_xGa_{1-x}N$/GaN DQWs and the *M*-plane background of the sample.

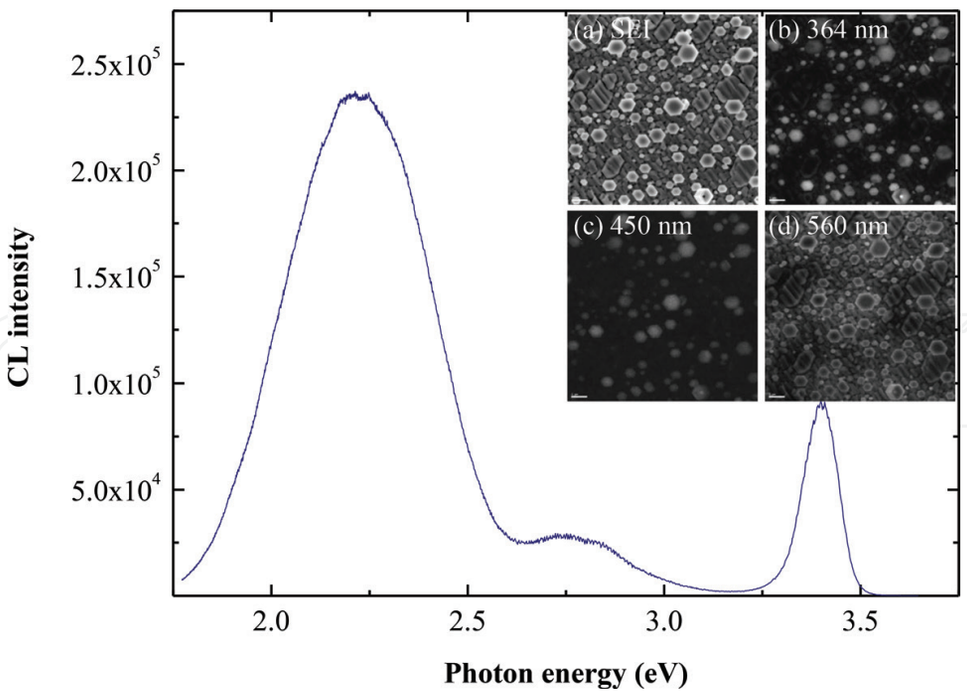

Figure 9. The CL spectrum measured at room temperature for the $In_xGa_{1-x}N$/GaN QW of the sample. The inset (a) shows the SEM image. The inserts (b), (c) and (d) show the CL images for wavelength of 364 nm, 433 nm, and 550 nm to the peak energies of CL spectrum.

The microstructure of the $In_xGa_{1-x}N$/GaN microdisk sample was analysed by field emission transmission electron microscopy (FE-TEM) (Phillips, model Tecnai F-20) with an electron voltage of 200 kV. The cross-sectional TEM specimen of the sample was prepared by a dual-beam FIB system (Seiko Inc., SII-3050), on the cleavage plane along the $[1\bar{1}\,0\,0]$ direction of the *c*-plane GaN hexagonal microdisk. The FIB was performed with an accelerated voltage of 30 kV to cut the samples roughly and then refined the specimen further by an accelerated voltage of 5 kV. **Figure 10(a)** and **(b)** shows the bright field image with the $[1\,1\bar{2}\,0]_{GaN}$ // $[0\,0\,1]_{LAO}$ zone axis, and we found that the height of the microdisk is about 2.12 μm. **Figure 10(c)** shows the scanning transmission electron microscopy (STEM) images of the $In_xGa_{1-x}N$/GaN MQWs grown on the GaN microdisk. From the high contract image between $In_xGa_{1-x}N$ wells and GaN barriers, as shown in **Figure 10(f)**, the thicknesses of $In_xGa_{1-x}N$ well and GaN barrier evaluated from the STEM image were found to be about 2.75 and 17 nm, respectively. The quantum-well-thickness of 2.75 nm offers a good quantum confinement for the charged carriers and photon emission in the $In_xGa_{1-x}N$/GaN DQWs. It is consistent with the results of PL and CL spectra. The selective area diffraction (SAD) pattern at the top area of GaN microdisk shown in **Figure 10(d)** clearly showed one single rectangular diffraction pattern at the location of DP01, indicating that the hexagonal microdisk was uniquely formed by the ***c***-plane wurtzite GaN. The ***d***-spacing between the $\{0\,0\,0\,\bar{1}\}$ planes of GaN hexagonal microdisk was measured to be d_c = 0.5172 nm and the ***d***-spacing between the $\{1\bar{1}\,0\,0\}$ planes of GaN hexagonal

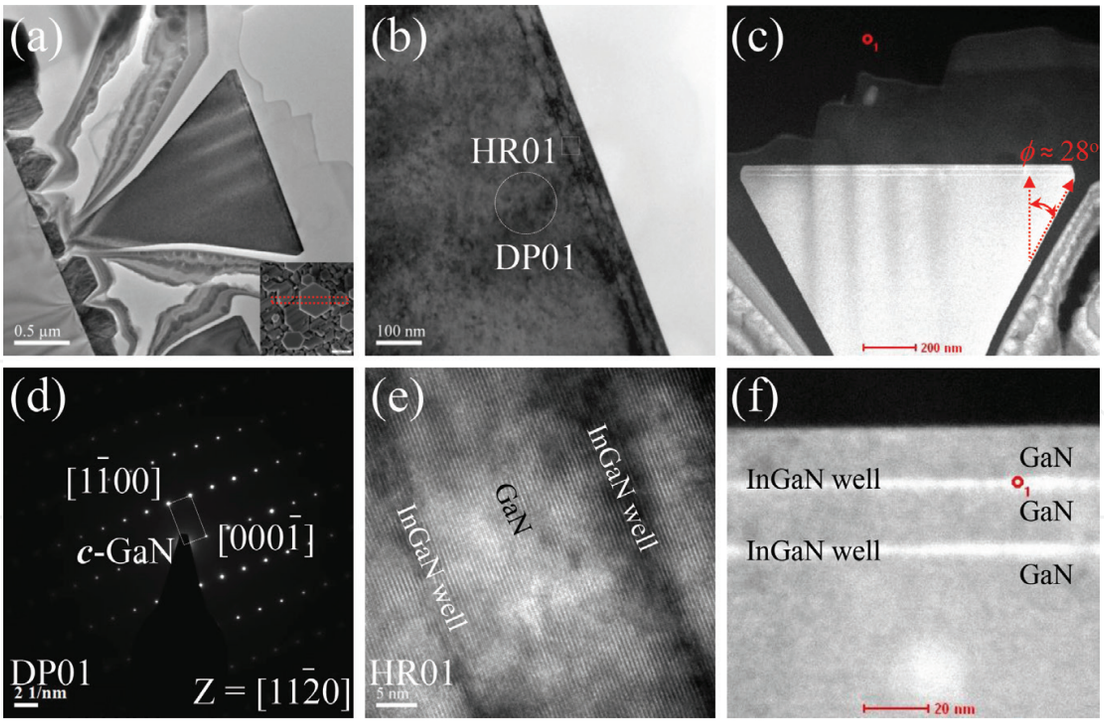

Figure 10. TEM analyses of the InGaN/GaN QW microdisk: (a) and (b) show the bright field images with $[1\ 1\ \bar{2}\ 0]_{GaN}$ // $[0\,0\,1]_{LAO}$ zone axis, the scale bars are 0.5 and 100 nm, respectively. (c) The STEM image taken at the top area of InGaN/GaN QW, the scale bar is 200 nm. The selective area diffraction patterns taken at the points shown in (b) are presented in (d), the scale bar is 2 (1/nm). The high-resolution TEM images taken at the point shown in (b) are presented in (e), the scale bars are 2 nm. (f) The enlarged STEM image of InGaN/GaN QW (the scale bar is 20 nm).

microdisk was d_M = 0.2764 nm. The angle between edge and growth direction can be obtained by $\phi = \tan^{-1}(d_M/d_c) = 28.1°$, which was in good agreement with the model predicted. The angle between the edge and the growth direction examined directly by the STEM image can be found about 28°, as shown in **Figure 10(c)**. The high-quality crystalline micro structures for the $In_xGa_{1-x}N$/GaN DQWs were reconfirmed by the high-resolution TEM images, as shown in **Figure 10(e)**. It showed that the $In_xGa_{1-x}N$ wells were well-stacked on the high-quality GaN microdisk to form well-assembled crystalline $In_xGa_{1-x}N$/GaN DQWs with some minor structural defects (e.g. dislocations or stacking-faults) occurred in the $In_xGa_{1-x}N$ wells. The HR results indicated that the density of structural defects in $In_xGa_{1-x}N$ wells is greater than that in GaN layers. It supported the results of FWHM analyses of PL spectra, indicating that FWHM (0.173 eV) for the peak of 2.192 eV from $In_xGa_{1-x}N$ wells was greater than FWHM (0.043 eV) for the peak of 3.383 eV from the wurtzite GaN layer. The structural defeats in $In_xGa_{1-x}N$ wells yield the peak of 2.805 eV in CL measurement.

5. Conclusion

We have grown GaN and InN hexagonal microdisks on the LAO substrates at low temperatures (GaN at 630°C and InN at 470°C) by PA-MBE. From the SEM images and TEM analyses, we found that 3D ***c***-plane hexagonal microdisks and 2D ***M***-plane epi-film were grown on the LAO substrate. From TEM analyses, the oblique angle of GaN and InN hexagonal microdisks can be examined directly to be about 28 and 73°, respectively. The lateral over-growth mechanism causes the bigger oblique angle of InN hexagonal thin disks at low growth temperature. From PL and CL analyses, we found that the high-intensity light of 367-nm wavelength (3.380 eV) and 566-nm wavelength (2.192 eV) emitted from the GaN microdisks and $In_xGa_{1-x}N$/GaN quantum wells, respectively. Therefore, the stain-free microdisk provides an opportunity to fabricate $In_xGa_{1-x}N$/GaN microdisk quantum well for the application of full-colour micron LED without the sapphire substrate.

Acknowledgements

The project was supported by the Ministry of Science and Technology of Taiwan and the Core Facilities Laboratory for Nanoscience and Nanotechnology in Kaohsiung and Pintung Area.

Author details

Chen-Chi Yang, Ikai Lo*, Yu-Chi Hsu and Hong-Yi Yang

*Address all correspondence to: ikailo@mail.phys.nsysu.edu.tw

Department of Physics, Center for Nanoscience and Nanotechnology, National Sun Yat-Sen University, Kaohsiung, Taiwan

References

[1] Nakamura S, Senoh M, Iwasa N, Nagahama SI, Yamada T, Mukai T. Superbright green InGaN single-quantum-well-structure light-emitting diodes. Japanese Journal of Applied Physics. 1995;**34**(Part 2, Number 10B):L1332-L1335. DOI: 10.1143/JJAP.34.L1332

[2] Nakamura S, Pearton S, Fasol G, editors. The Blue Laser Diode. 2nd ed. The Complete Story. Springer ed. Berlin: Springer Science & Business Media; 2000. p. 367. DOI: 10.1007/978-3-662-04156-7

[3] Lo I, Tsai JK, Yao WJ, Ho PC, Tu LW, Chang TC, Elhamri S, Mitchel WC, Hsieh KY, Huang JH, Huang HL, Tsai WC. Spin splitting in modulation-doped $Al_xG_{a1-x}N$/GaN heterostructures. Physics Review B. 2002;**65**(16):161306. DOI: 10.1103/PhysRevB.65.161306

[4] Lo I, Wang WT, Gau MH, Tsai JK, Tsay SF, Chiang JC. Gate-controlled spin splitting in GaN/AlN quantum wells. Applied Physics Letters. 2006;**88**:082108. DOI: 10.1063/1.2178505

[5] Lo I, Hsieh CH, Hsu YC, Pang WY, Chou C. Self-assembled GaN hexagonal micropyramid and microdisk. Applied Physics Letters. 2009;**94**:062105. DOI: 10.1063/1.3079078

[6] Fred Schubert E, Kim JK. Solid-state light sources getting smart. Science. 2005;**308**(5726): 1274-1278. DOI: 10.1126/science.1108712

[7] Ponce FA, Bour DP. Nitride-based semiconductors for blue and green light-emitting devices. Nature. 1997;**386**(6623):351-359. DOI: 10.1038/386351a0

[8] Vurgaftman I, Meyer JR. Band parameters for nitrogen-containing semiconductors. Journal of Applied Physics. 2003;**94**:3675. DOI: 10.1063/1.1600519

[9] Madelung O, editor. Semiconductors: Group IV Elements and III–V Compounds. New York: Spring; 1991. p. 163. DOI: 10.1007/978-3-642-45681-7

[10] El-Masry NA, Piner EL, Liu SX, Bedair SM. Phase separation in InGaN grown by metalorganic chemical vapor deposition. Applied Physics Letters. 1998;**72**:40. DOI: 10.1063/1.120639

[11] Tsai JK, Lo I, Chuang KL, Tu LW, Huang JH, Hsieh CH, Hsieh KY. Effect of N to Ga flux ratio on the GaN surface morphologies grown at high temperature by plasma-assisted molecular-beam epitaxy. Journal of Applied Physics. 2004;**95**:460. DOI: 10.1063/1.163438895: 460

[12] Lo I, Wang YC, Hsu YC, Shih CH, Pang WY, You ST, Hu CH, Chou MMC, Hsu GZL. Electrical contact for wurtzite GaN microdisks. Applied Physics Letters. 2014;**105**(8): 082101. DOI: 10.1063/1.4894080

[13] Hsieh CH, Lo I, Gau MH, Chen YL, Chou MC, Pang WY, Chang YI, Hsu YC, Sham MW, Chiang JC, Tsai JK. Self-assembled c-plane GaN nanopillars on γ-$LiAlO_2$ substrate grown by plasma-assisted molecular-beam epitaxy. Japanese Journal of Applied Physics. 2008;**47**(2R):891. DOI: 10.1143/JJAP.47.891

[14] Lo I, Hsieh CH, Chen YL, Pang WY, Hsu YC,Chiang JC, Chou MC, Tsai JK, Schaadt DM. Line defects of M-plane GaN grown on g-$LiAlO_2$ by plasma-assisted molecular beam epitaxy. Applied Physics Letters. 2008;**92**:202106. DOI: 10.1063/1.2924288

[15] Reshchikov MA, Morkoc HJ. Luminescence properties of defects in GaN. Journal of Applied Physics. 2005;**97**:061301. DOI: 10.1063/1.1868059

[16] Yang CC, Lo I, Hu CH, Huang HC, Chou MMC. Growth of InN hexagonal microdisks. AIP Advances. 2015;**6**:085015. DOI: 10.1063/1.4961699

[17] Denton AR, Ashcroft NW. Vegar's law. Physical Review A. 1991;**43**(6):3161. DOI: 10.1103/PhysRevA.43.3161

[18] Hsu YC, Lo I, Shih CH, Pang WY, Hu CH, Wang YC, Tsai CD, Chou MMC, Gary Z. Green light emission by InGaN/GaN multiple-quantum-well microdisks. Applied Physics Letters. 2014;**104**:102105. DOI: 10.1063/1.4868417

[19] Vegard L. Die Konstitution der Mischkristalle und die Raumfüllung der Atome. Zeitschrift Fur Physik. 1921;**5**:17-26. DOI: 10.1007/BF01349680

[20] Choi S, Ton-That C, Phillips MR, Aharonovich I. Observation of whispering gallery modes from hexagonal ZnO microdisks using cathodoluminescence spectroscopy. Applied Physics Letters. 2013;**103**:171102. DOI: 10.1063/1.482648s1